RESEARCH PAPER

IntraVital 4:2, e1066949; May/June/July/August 2015; Published with license by Taylor & Francis Group, LLC

A novel model for ectopic, chronic, intravital multiphoton imaging of bone marrow vasculature and architecture in split femurs

Mirela Bălan[1,2,3] and Friedemann Kiefer[1,2,*]

[1]Mammalian Cell Signaling Laboratory; Max Planck Institute for Molecular Biomedicine; Münster, Germany; [2]Cluster of Excellence; Cells in Motion, CiM; Münster, Germany; [3]Current address: Division of Vascular Biology; Department of Medical Biochemistry and Biophysics (MBB); Karolinska Institute; Stockholm, Sweden

Keywords: chronic imaging model, dorsal skinfold chamber, ectopic transplantation, femoral bone marrow imaging, intravital imaging, imaging window, split femur, two photon microscopy

Abbreviations: BM, bone marrow; BV, blood vessels; CFU, colony forming unit; DSC, dorsal skinfold chamber; DsRed, *Discosoma* sp. red fluorescent protein; EC, endothelial cells; EMCN, endomucin; GFP, green fluorescent protein; HC, haematopoietic cells; MIP, maximum intensity projection; OPN, osteopontin; P, postnatal day; PI, propidium iodide; RFP, red fluorescent protein; SHG, second harmonic generation; SOC, secondary ossification center.

Creating a model for intravital visualization of femoral bone marrow, a major site of hematopoiesis in adult mammalian organisms, poses a serious challenge, in that it needs to overcome bone opacity and the inaccessibility of marrow. Furthermore, meaningful analysis of bone marrow developmental and differentiation processes requires the repetitive observation of the same site over long periods of time, which we refer to as chronic imaging. To surmount these issues, we developed a chronic *intravital* imaging model that allows the observation of split femurs, ectopically transplanted into a dorsal skinfold chamber of a host mouse. Repeated, long term observations are facilitated by multiphoton microscopy, an imaging technique that combines superior imaging capacity at greater tissue depth with low phototoxicity. The transplanted, ectopic femur was stabilized by its sterile environment and rapidly connected to the host vasculature, allowing further development and observation of extended processes. After optimizing transplant age and grafting procedure, we observed the development of new woven bone and maturation of secondary ossification centers in the transplanted femurs, preceded by the sprouting of a sinusoidal-like vascular network, which was almost entirely composed of femoral endothelial cells. After two weeks, the transplant was still populated with stromal and haematopoietic cells belonging both to donor and host. Over this time frame, the transplant partially retained myeloid progenitor cells with single and multi-lineage differentiation capacity. In summary, our model allowed repeated intravital imaging of bone marrow angiogenesis and hematopoiesis. It represents a promising starting point for the development of improved chronic optical imaging models for femoral bone marrow.

Introduction

Femoral bone marrow (BM) is a major site of hematopoiesis, which crucially depends on the structural composition and histological architecture of the BM. This unique cellular environment, often referred to as the niche, enables and supports BM function and directs hematopoiesis.[1] A large body of evidence suggests that disturbance of this complex 3-dimensional arrangement will impair its regulatory functions and lead to the development of pathologies.[2] However, direct microscopic evidence for this assumption is scarce. The intravital microscopic interrogation of the femoral BM architecture and function is severely limited by its encasing in opaque bone.

Being central for posture and locomotion, generation of direct optical access to femoral BM by surgical thinning or removal of bone is only possible for limited periods of time, that preclude the analysis of developmental and differentiation processes.[3] Furthermore, the rapid environmental changes caused by surgery, such as the alteration in oxygenation status upon exposure of the bone marrow, together with the acute post-surgical trauma, may significantly alter the behavior of BM cells.

*Correspondence to: Friedemann Kiefer; Email: fkiefer@mpi-muenster.mpg.de
Submitted: 03/06/2015; Revised: 06/15/2015; Accepted: 06/18/2015
http://dx.doi.org/10.1080/21659087.2015.1066949

One alternative approach is imaging of the calvarial BM, which is significantly more accessible, and the extrapolation of the resulting observations to the femoral marrow. While valuable data have been obtained by this approach,[4-6] it has remained controversial how representative calvarial BM is for other BM compartments.[7] Therefore, we aimed to create a model that for the first time allows long-term direct optical imaging of femoral BM, which we refer to as chronic BM imaging.

Our approach was based on the assumption that a dorsal skin-fold chamber (DSC), which is surgically implanted on the back skin of a mouse,[8] could be used as a long-term transplantation and observation site for a split femur, as previously femoral bone transplants have been shown to be vascularized and to grow after transplantation into a DSC.[9-11] Indeed, we report here that the DSC provides a sterile and non-inflammatory environment that allows the rapid revascularization of a transplanted split femur and partial survival of BM cells in this graft. Analysis of the newly forming vasculature from the transplant revealed a strong resemblance with the vasculature of femoral bone marrow, providing evidence for organotypic vessel formation. Subsequently, this transplantation model enabled direct observation of the changes in vascularity and cellular composition of the BM in a femoral transplant.

Results

Transplantation of a split femur into a dorsal skin fold chamber is followed by rapid vascularisation

In this study, we aimed to develop a long-term imaging model for the vasculature and tissue architecture of femoral bone marrow. To overcome the inherent barrier of the opaque femoral bone, we decided to transplant a split femur into an ectopic, optically accessible position. For the femoral bone, we choose a splitting plane parallel to the greater trochanter and the femoral head to assure ideal optical access during later imaging (**Fig. 1A**).

As an optically accessible location for ectopic transplantation, we elected the dorsal skin-fold chamber (DSC), which is well established and excellently tolerated by rodents.[12] After surgical application of a DSC, we allowed the mice to recover for 2 days and then used only those animals without any signs of inflammation or post-surgical tissue damage as transplant recipients on the third day after chamber implantation (**Fig. 1D**). Femurs were isolated from newborn mice, split as shown (**Figs. 1B, C**). To stabilize the explanted femur during the splitting process and ensure perfect orientation of the splitting plane, we fixed the bone explants in a custom parallel vice during initial experiments. Subsequently, since we noted that splitting femurs with a scalpel while being held with watchmaker forceps was highly reproducible and provided indistinguishable results from the custom-made vice, we exclusively settled on this faster variant. After removal of the coverslip from the DSC, the split femur was placed in the chamber with the cut surface facing a newly applied sterile coverslip (**Fig. 1E**). After resealing of the chamber, the status of the transplant was recorded and animals were observed twice daily using a stereomicroscope. In more than 70 transplants, we did not observe free erythrocytes outside the vasculature immediately after transplantation (**Fig. 1E**). Reproducibly, we observed the accumulation of erythrocytes in the transplant, starting between 24 and 48 hrs after transplantation and covering the whole split surface within 4 days after transplantation. We also noted the onset of active perfusion of the transplant as indicated by a constant flow of erythrocytes in selected vessels within the transplant. Hematoma formation in and around the transplant was highly prominent by 4 d following transplantation (**Fig. 1F**). Concomitantly, we observed sprouting of blood vessels from the transplant toward the surrounding host tissue (**Fig. 1G**). As the newly forming vasculature elongated and ramified the hematoma-like accumulation of erythrocytes gradually disappeared (**Fig. 1H**), leading to the establishment of a new functional BM vasculature by 8 days after transplantation. This angiogenic process finally resulted in a new dense vascular network that covered the transplant and its immediate surroundings by 2 weeks after transplantation (**Fig. 1I**, asterisk). During this period of establishment of the new vasculature, starting as early as 5 days after transplantation, we injected various contrasting agents to observe vessel morphology, however, we did not detect obvious vascular discontinuities at any time point. Fluorescent dextran e.g. only slowly extravasated and was taken up by phagocytic cells in the transplant (Supplemental movie 1).

The development of split femurs after transplantation depends on donor age

To optimize our chronic BM imaging model, we tested the developmental potential and fate of split femurs from donors at different ages. We excluded adult donors on the basis of bone size and decreased age-related haematopoietic activity, and therefore tested femurs isolated from neonates between 5 and 17 days of age.

P05 femurs (isolated from 5 d old pups) were characterized by few and short trabeculae near the growth plate and the absence of a secondary ossification center (SOC) (**Fig. 2A**), which starts forming around P07, when the cartilage canal is formed from the perichondrium.[13] Split P05 femurs rapidly vascularized, however, immunofluorescence analysis revealed that the transplanted BM cavity filled with newly forming woven bone, which displaced the haematopoietic compartment (**Fig. 2B**). Interestingly, we noted in a P05 femur recovered 12 d after transplantation the invasion of osteopontin^{+} (OPN^{+}) cells into the epiphysis, indicative of the first steps of residual development of a SOC.

Because also P10 split femurs suffered from extensive ossification of the BM cavity after transplantation (**Fig. S1**), we analyzed the behavior of older P17 split femurs, in which the SOC is more developed, occupying most of the epiphysis, and the trabecular bone has extended into the primary ossification center (**Fig. 2C**). Two weeks after transplantation, we observed persistence of an open BM cavity alongside development of trabecular bone (**Fig. 2D**). Overall the appearance of a transplanted P17 split femur was similar enough to a P31 femur (**Fig. 2E**) therefore we decided to use P17 for further transplantation experiments. We

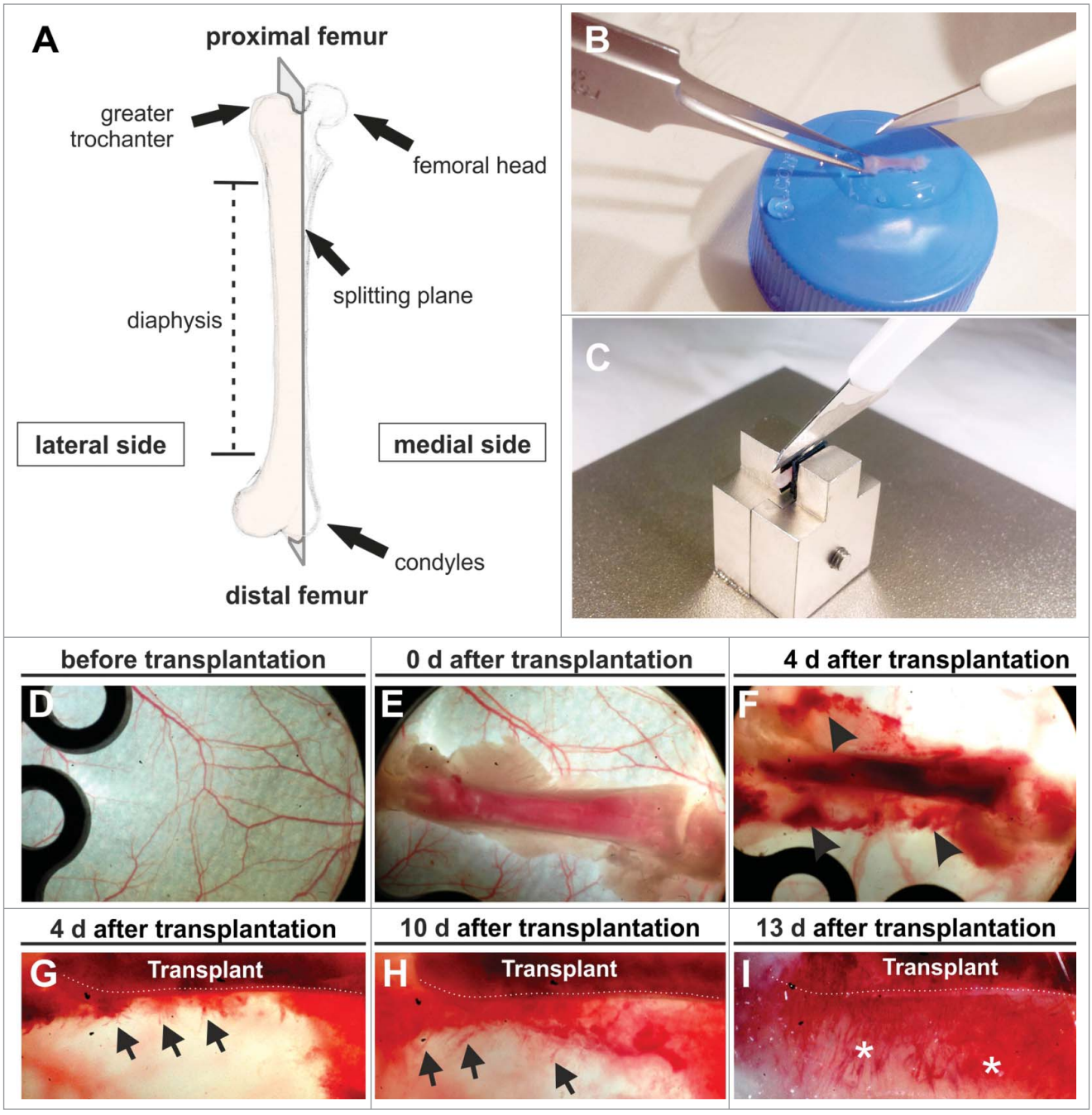

Figure 1. Rapid vascularisation of split femurs after transplantation into a dorsal skin-fold chamber (DSC). (**A**) Cartoon depicting the selected plane for splitting neonatal femurs to optimize imaging after transplantation. (**B**) Femurs were immobilized either with a forceps or (**C**) using a custom-made miniature parallel vice before being split with a scalpel blade. (**D**) Only DSCs free of signs of inflammation or damage were used for the transplantation of split femurs. (**E**) View of the split femur immediately after transplantation. (**F**) Four days after transplantation prominent erythrocyte accumulations were observed over the entire transplant (black arrowheads) and (**G**) stereomicroscopic inspection revealed sprouting of blood vessels from the bone shaft (black arrows). (**H**) Within the next week the sprouting front (black arrows) expanded into the host environment. (**I**) Two weeks after transplantation an extensive vascular network (asterisks) connected the graft to the surrounding skin. Dotted white line denotes the edge of the transplanted split femur, position of the transplant is indicated. The splitting plane was maintained throughout more than 70 transplantations performed.

noted that the expansion of trabecular bone had progressed since the time of transplantation, however, lagged behind the age matched control (**Fig. S2**). BVs were present in the marrow cavity although they were less densely packed and had a larger diameter.

The newly formed vascular network originates largely from the femoral vasculature

The observation of sprout formation from the edge of the transplant suggested that the newly forming vascular network may have largely originated from the transplant. To distinguish

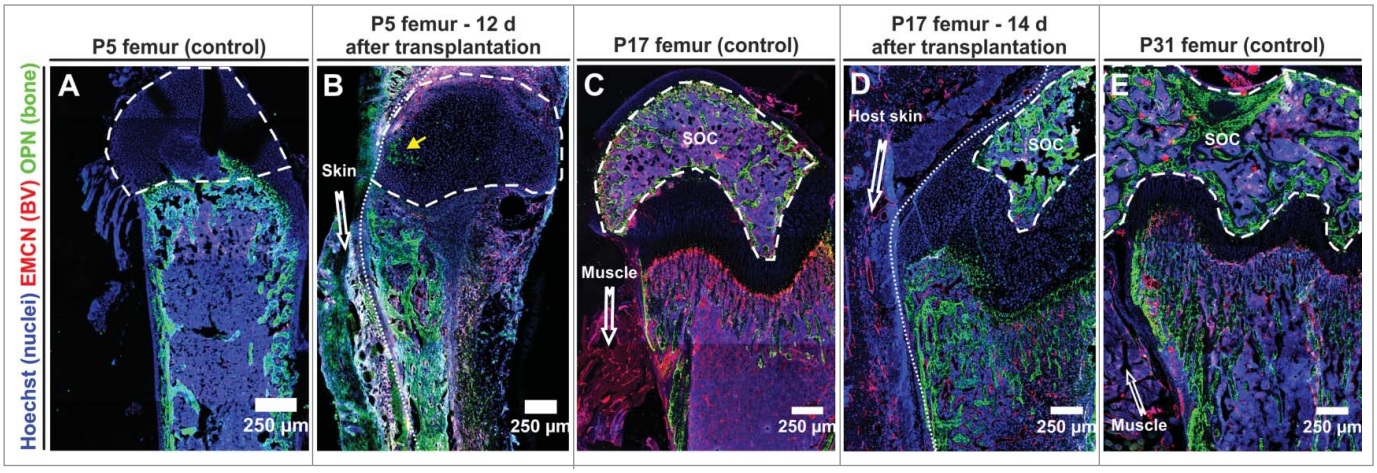

Figure 2. The developmental fate of transplanted femurs strongly depends on the age of the graft at the time of transplantation. (**A, C, E**) Representative control immunofluorescence staining of neonatal femurs at the indicated age (P5, P17, P31) – 3 femurs per age category. (**B**) 12 days after transplantation of a P5 femur the bone marrow cavity was largely filled with new woven bone secreted by OPN^+ cells. OPN^+ cells were also seen to invade the epiphysis (yellow arrow). Representative figures obtained from 2 transplants. (**D**) Femurs collected from P17 pups maintained their open BM cavity for 14 days after transplantation and reached a developmental stage that was reminiscent of a P31 control femur. Representative figures from 4 transplants. (**E**). Compared to the age matched control (**E**), development of the secondary ossification center (SOC) in the transplanted femur was delayed. All panels depict 8 μm cryosections that were analyzed by confocal microscopy (tile-scan). Dashed line encircles the SOC, dotted line demarks border transplant host, EMCN endomucin, BV blood vessel, OPN osteopontin.

the contribution of transplant and host to neo-vessel formation, we took advantage of genetically labeled mouse lines. We transplanted split femurs from mice expressing a LifeAct-GFP transgene into recipients, in which the endothelial and a large part of the myeloid compartment were labeled by Tie2-Cre driven tdRFP expression from the Rosa26 locus.

In this constellation, most of the dense vascular network overlaying the transplant originated from the transplant (**Fig. 3A**). While it was amply surrounded by $tdRFP^+$ cells, we noted a remarkable absence of $tdRFP^+$ BVs either in, overlaying or in close proximity to the transplanted femur (**Fig. 3B**). Newly sprouting GFP^+ BVs arose from the dense vascular plexus in the marrow (**Fig. 3C**), crossed the bone shaft (**Fig. 3C**, dashed white lines) and then split into smaller BVs, which ultimately created a dense network which was functionally connected with the host environment (**Fig. 3C**, asterisk). In few instances, we were able to observe instances of anastomosis between transplant and host-derived endothelial cells (**Figs. 3, D–F**).

Newly forming vessels bear morphologic resemblance to the femoral vasculature

Different vascular beds show distinct functional characteristics of the endothelium (**Figs. 4A and F**). The finding that the overwhelming majority of newly formed vessels arose by sprouting from the transplant raised the question if these might recapitulate aspects of the bone marrow vasculature. Presently, there are no specific surface markers known that would be unique to BM sinusoidal vessels, hence we had to base our analysis largely on morphological criteria. To address this issue, we performed overview immunostainings of the endothelial sialomucin endomucin, which is most strongly expressed on the surface of microvascular and venous endothelial cells.[14,15] We noted significant differences in branching pattern, density and morphology between the vessels within or adjacent to a transplant that had been grafted 20 days earlier, and the vasculature of the host (**Fig. 4A**). For this analysis, we purposefully allowed a long 20 d lapse between transplantation and observation to identify morphological properties that remained stable after vascularization.

Subsequent intravital multiphoton imaging using either quantum dots (**Fig. 4C**) or FITC-dextran (**Fig. 4D**) as a contrasting agent confirmed these differences in morphology. While host vessels underneath or within the panniculus carnosus inside the chamber were smooth, thin, with rare branching points and no vascular loops (**fig. 4D**), the newly generated vessels overlaying the BM were of generally thicker and more variable diameter and appeared more chaotic, with frequent branching points that made quantification unpractical (**Figs. 4 C, J**). A layer analysis revealed various vascular loops overlapping in different layers of the preparation (**Figs. 4G, H** white arrows). Furthermore, the newly formed vessels displayed frequent vascular openings / discontinuities, possibly indicative of vessel fusion (**Fig. 4 G, H, I** yellow arrows) and abundant filopodia (**Fig. 4 G, H, I** white asterisks). Also, when we compared the median filopodial length of the transplant vessels and the normal femoral BM vasculature, we detected no significant difference (**Fig. S3**).

Taken together, the transplant BVs were highly reminiscent of the BVs in the BM of a P17 control neonate (**Figs. 4 E, F**), but very different from the host vessels of the muscular environment

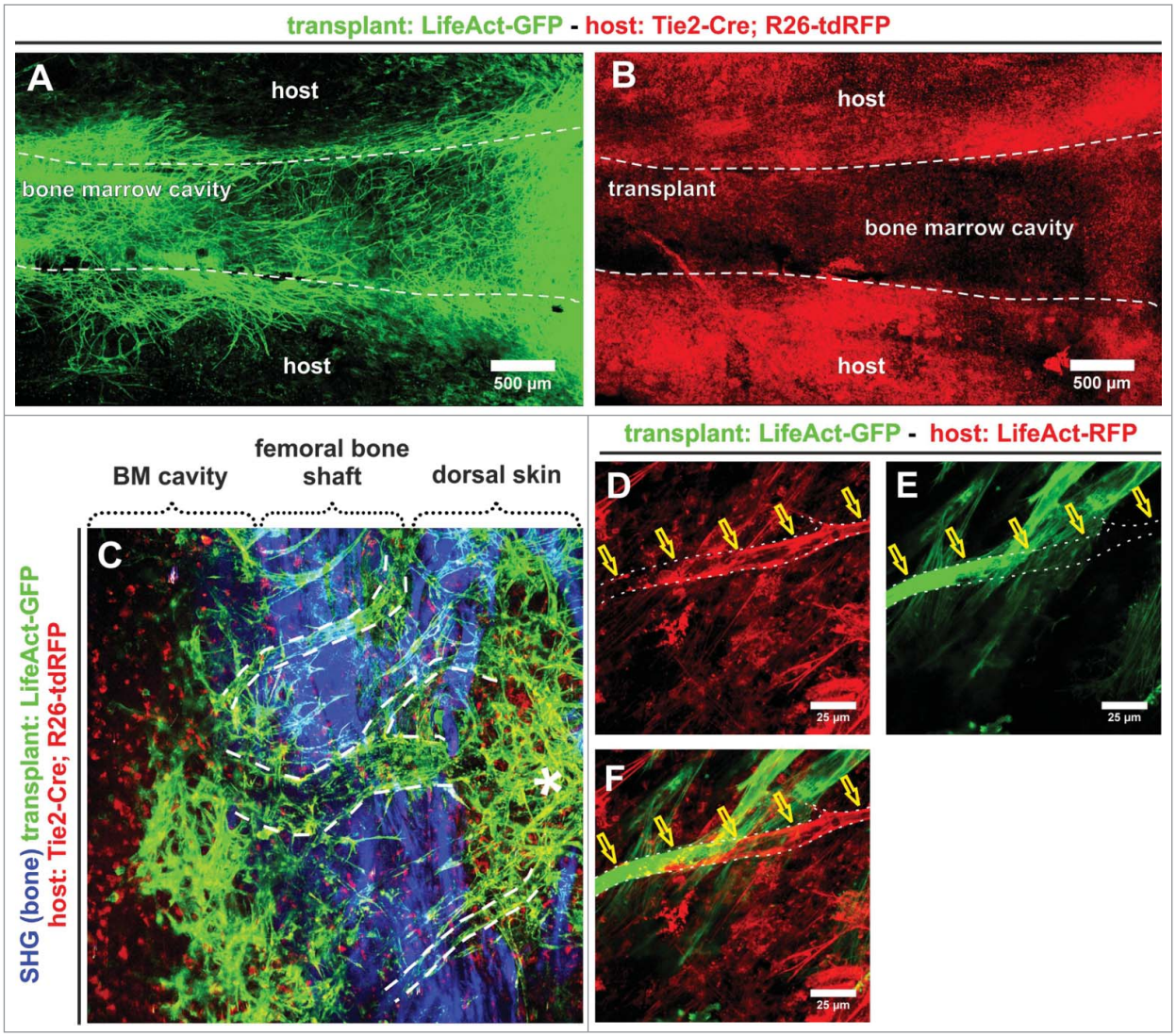

Figure 3. Genetic marking reveals the formation of an extended vascular network by transplanted split femurs. (**A**) Transplantation of P17 split femurs from LifeAct-GFP mice revealed extensive sprouting and vessel formation from the transplant, while (**B**) vascularisation of the transplant by host vessels was extremely rare, and not visible in an overview of the transplant. (**A, B**) Confocal tile-scan of a whole mount split femur (LifeAct-GFP^{+}) transplanted into a Tie2-Cre;R26-tdRFP host. (**C–F**) 27 days after transplantation, the newly formed transplant-derived vessel plexus extends well beyond the transplant borders and anastomoses between the host and transplant-derived vessels. (**C**) Dashed lines in maximum intensity projection (MIP) of multiphoton image stack, denote vessels crossing the transplant border, asterisk indicates part of the transplant-derived plexus that is located outside of the transplant. (**D–F**) Anastomosing vessels (indicated by yellow arrows) were infrequently observed outside the transplant. Vessel is delineated by the white dashed line. The observations were confirmed in 3 separate whole mount transplants.

(**Figs. 4D, F**). The fact that the overall distribution and diameter of the BVs in the transplant varied from bona fide femoral BVs probably resulted from the extensive sprouting and remodeling processes in the newly established plexus.

The newly formed vasculature is associated with NG2^{+} perivascular cells

Perivascular cells fulfill important roles in stabilizing blood vessels and regulating blood flow. They also engage in reciprocal interactions with the vascular endothelium, which are important for organ specific endothelial differentiation.[16]

We wondered to which extend the new vascular plexus sprouting from the transplant was invested by perivascular cells and therefore used the NG2-DsRed mouse line. In this transgenic model, NG2^{+} perivascular and mesenchymal stromal cells are labeled by NG2 promotor-driven DsRed expression. Ten days after transplantation, we readily identified NG2^{+} cells within the BM cavity (**Figs. 5A,B**) and the cortical bone of the femoral shaft (**Fig. 5A**). NG2^{+} perivascular cells frequently lined blood vessels and those associated with the largest vessels displayed the tendency to wrap the vessel in parallel orientation rectangular to the direction of flow (**Fig. 5B**).

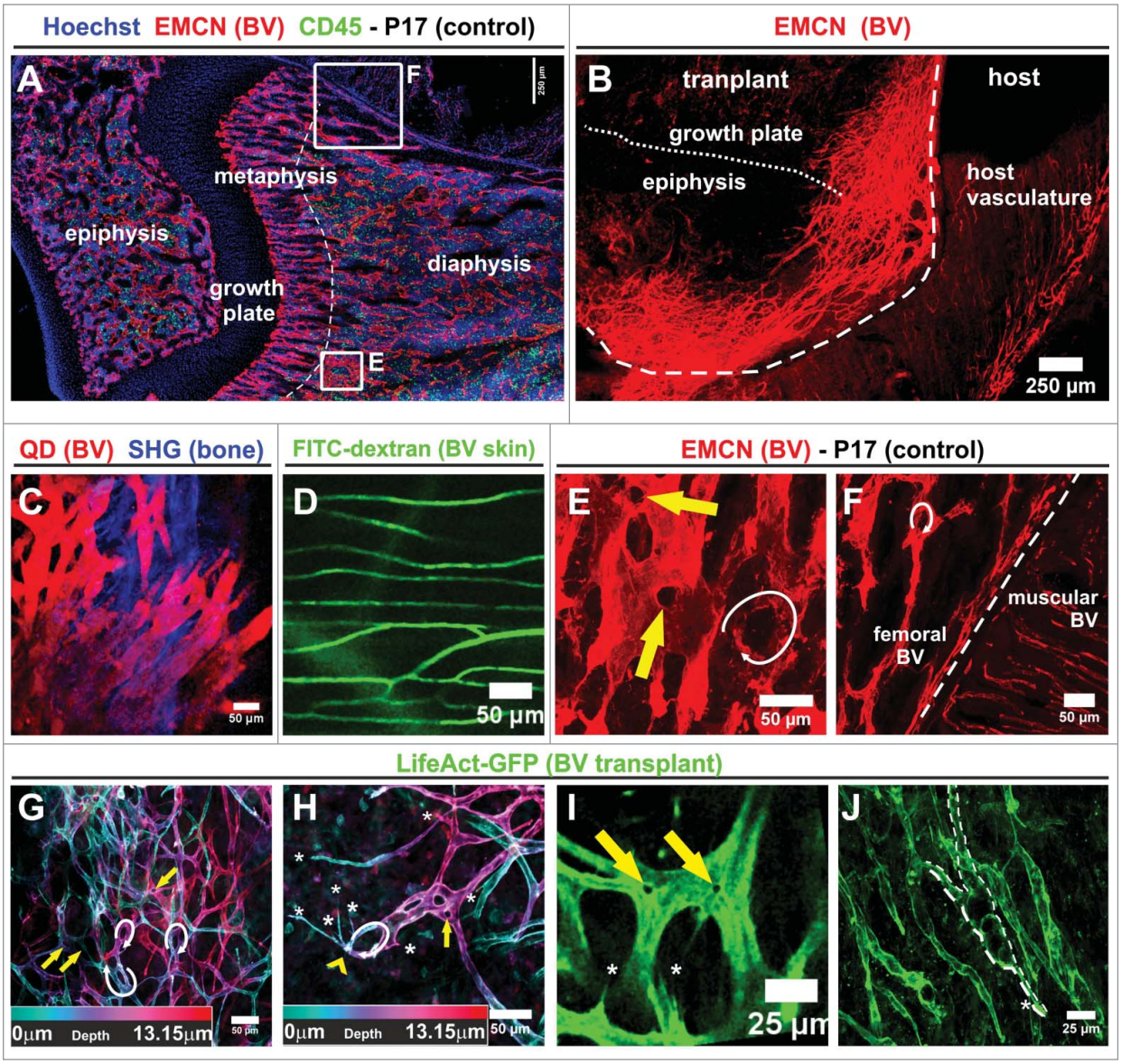

Figure 4. The morphology of new blood vessels, sprouting from split femur transplants, differs significantly from the skin vasculature. (**A**) Immunofluorescence whole mount staining of a P17 femur (control) to reveal BM and vascular architecture. The dotted line indicates the border between the metaphysis and diaphysis (representative slide from 4 femurs). (**B**) Immunofluorescence whole mount staining for endomucin 20 days after transplantation of a split femur (3 whole mounts). Dashed line delimits edge of the transplant, pointed line indicates the border between epiphysis and growth plate. (**A, B**) Confocal overview tile scan. (**C**) Intravital visualization of the nascent vascular network emerging from a P17 split femur 15 days after transplantation. Macoun Red quantum dots (QD) injected i.v. served as a contrasting agent, maximum intensity projection of a 108 µm image stack taken with a multiphoton microscope (representative of 2 injected transplants). (**D**) Vasculature of adjacent skin imaged 6 days after transplantation of a P17 split femur. The vascular lumen was contrasted by injection of FITC-dextran (in 2 observed chambers). (**C, D**) MIP of multiphoton image stacks. (**E, F**) Magnification of the indicated areas shown in the confocal overview tile scan in (**A**). Arrows denote prominent openings / discontinuities (yellow) and loops (white) characteristic of femoral BM vasculature. (**G, H**) Analysis of the spatial architecture of the newly forming vasculature in split transplants. Depth color-coding reveals the 3-dimensional organization. (**I,J**) Also more established vessels following the sprouting front retained the vascular openings / discontinuities characteristic of vascular fusion (yellow arrows in **G–I**) and loops (white arrows in **G–I**) frequently seen in the normal femoral vasculature (arrows in **E, F**) and their structure was reminiscent of the sinusoidal morphology. The newly forming vasculature presented sprouting filopodia (**H, I** labeled by white asterisks). (**G–J**) for these observations, 3 whole mount femurs were imaged.

NG2^{+} cells also covered the more established part of the newly formed plexus, where their cell bodies were tightly associated with the vasculature (**Fig. 5C**). Closer to the sprouting front, NG2+ cells displayed ample filopodia, were more loosely associated with and covered less of the endothelium. If the reduced coverage of the BVs by NG2+ cells results from mural cells following the sprouting front or if the NG2+ cells originate elsewhere, will need additional dynamic imaging of this transgene combination in transplanted femurs (**Fig. 5D**).

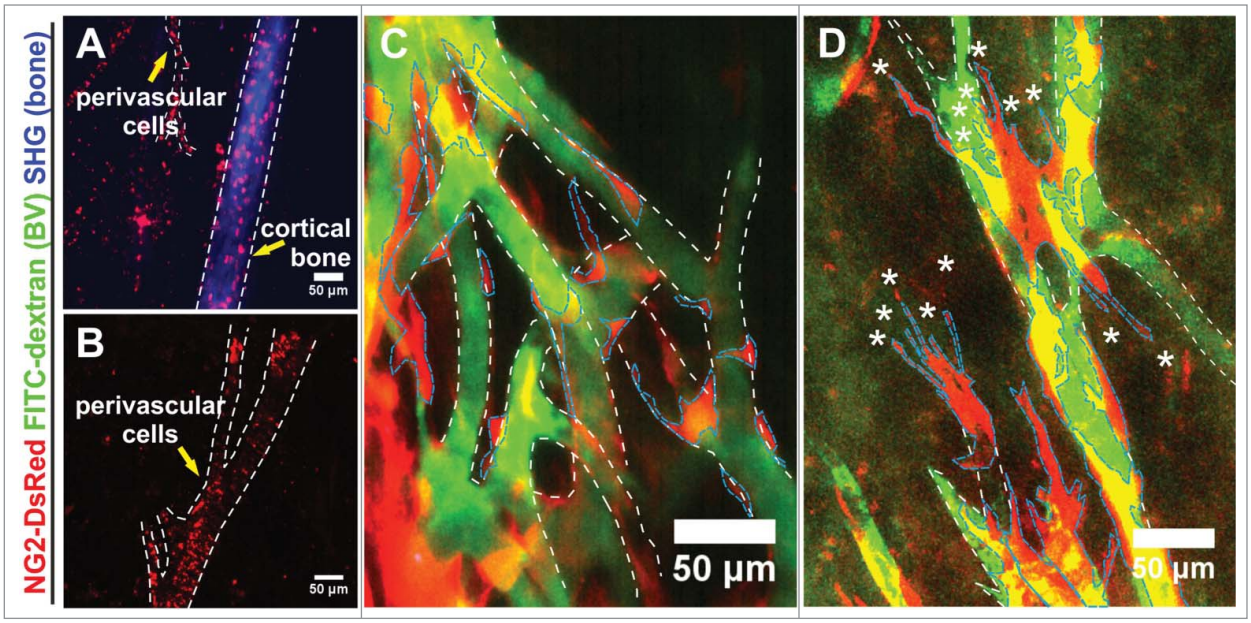

Figure 5. Distribution of NG2$^+$ cells in a transplanted split femur. (**A**, **B**) 10 days after transplantation, NG2-expressing cells marked by DsRed were prominent within the cortical bone (**A**) and lined BVs (demarked by white outline) without abundant ramifications of a split femur (**A**, **B**). (**C**) NG2$^+$ perivascular cells (demarked by blue outline) lined BVs (demarked by white outline) distant from the sprouting edge in an apparently stable association; (**D**) NG2$^+$ perivascular cells (blue outline) liaising with BVs (white outline) at the sprouting edge were characterized by multiple filopodia (asterisks) and an apparently loose association with the BVs. (**A–D**) MIPs of multiphoton image stacks, 4 transplants.

Split femurs provide sustainable access to image the dynamics of bone marrow angiogenic responses

As part of our characterization of the split femur model, we had defined a donor age and conditions that favored efficient reperfusion and development of an open BM cavity after transplantation of a split femur. Furthermore, we had shown that the newly forming vascular plexus was mostly derived from transplanted BM vessels and retained essential morphological characteristics of BM vasculature. We therefore tested the applicability of the split femur model for intravital imaging of the dynamic angiogenic response of vessels in the BM cavity. On average DSCs remained usable for imaging over 3 weeks after transplantation before they deteriorated due to mechanical load on the skin (also see supplementary Fig. 4). In contrast to local thinning of the calvarial or femoral bone,[3,4,6] the split femur allowed access at defined positions over the entire length of the BM cavity in a single imaging session, covering epiphyses, metaphyses and diaphysis. Using multiphoton microscopy, we were able to observe the transplant up to 400 µm under the level of the coverslip, but routinely acquired stacks covering typically 200 – 340 µm in the axial dimension, independently of the imaging position. Supplemental movie 2 shows a z-stack of 271 µm depth with a 1 µm step width, acquired from a LifeAct-GFP transplant in a LifeAct-RFP host at 3.5 days after transplantation. We started stack acquisition as close as possible to the level where the cortical bone signal is present to limit observation to the marrow that is present within the confines of the transplant, and continued in depth as far as we could acquire haematopoietic cell signals. Using time lapse microscopy, we were able to visualize typical angiogenic responses like the formation of novel vessel sprouts. Supplemental movie 3 shows a single imaging session covering 6 hours of a LifeAct-GFP expressing transplant that had been implanted 4 days earlier. Typical sprouting responses with filopodia extending tip cells were visible in 2 areas of the angiogenic front (indicated by red and yellow arrows correspondingly). To orient within the transplant, we used as anatomical landmarks the bone shaft and the relative distances to the epiphyses, which are readily visualized by 2nd harmonics generation.

Myeloid progenitor cells are retained in transplanted split femurs, however, total haematopoietic activity rapidly declines after transplantation

Contrasting of the perfused vasculature by i.v. injection of fluorescent dextran impenetrable to blood vessels demonstrated that the newly formed vascular plexus was well connected to the circulation and homogeneously perfused (**Figs. 4C, 5C,D**). Immunostaining of cyrosections of split femurs demonstrated abundant CD45$^+$ cells within the newly forming SOC and the BM cavity, suggesting the BM vasculature was capable of retaining haematopoietic cells after transplantation (**Fig. 6B**). We used genetically encoded fluorescent proteins to distinguish transplant and host derived cells. Because the kinase Syk is exclusively expressed in haematopoietic cells, but not in BM endothelium[17] transplantation into a Syk-Cre; R26-YFP host allowed the detection of host derived haematopoietic cells in a transplanted split femur, which comprised at least 10% of the haematopoietic cells (**Fig. 6C**).

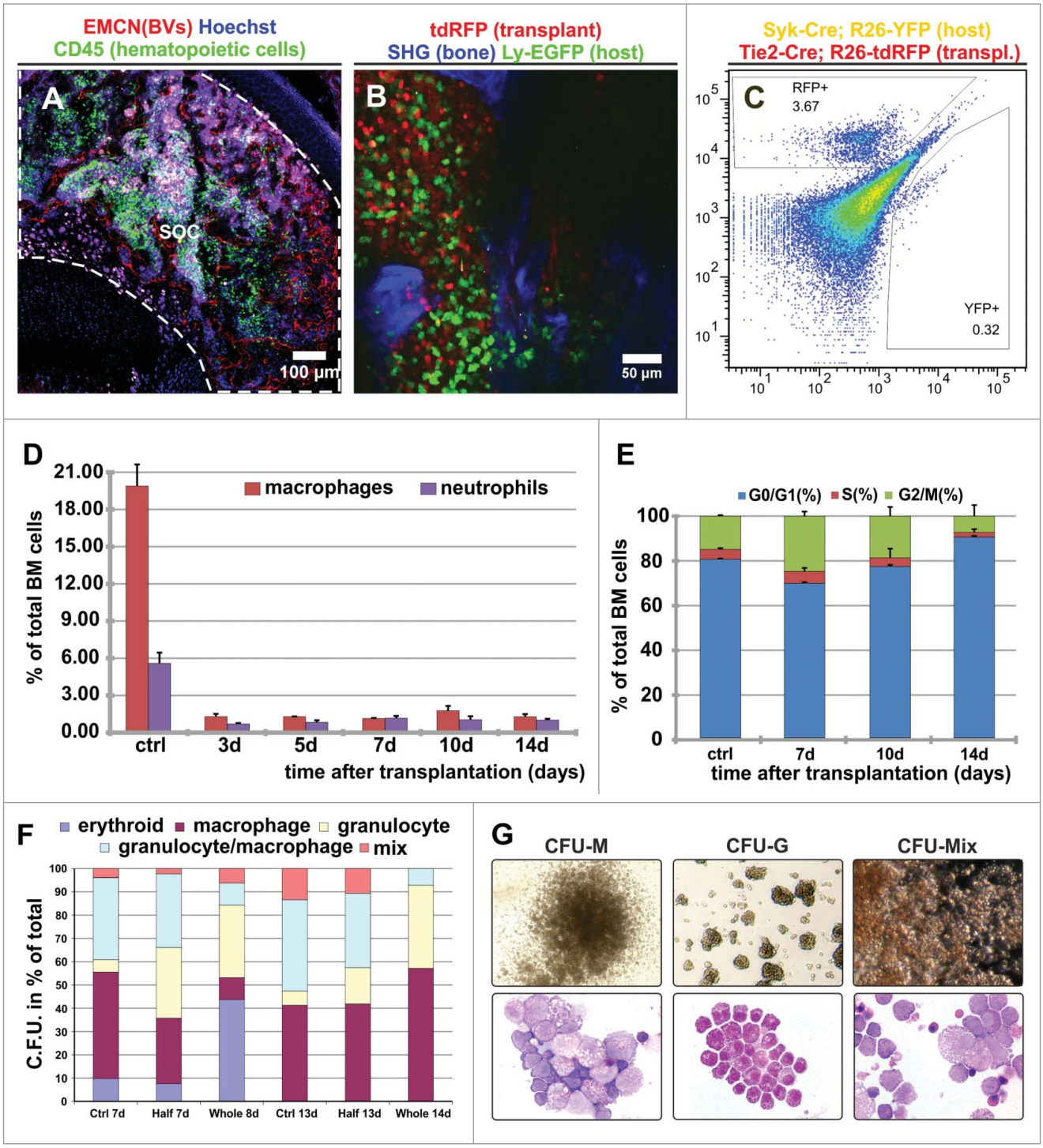

Figure 6. For figure legend, see page 9.

We noted a sharp decline in the number of haematopoietic cells during the first 3 days after transplantation to approx. 10% of the CD45+ cell present in a freshly split femur (**Fig. 6D**). Subsequently, the number of haematopoietic cells recovered slightly between 7 to 10 days after transplantation and then very gradually started to decline. Concomitantly, we detected a mild increase in proliferating cells (S and G2/M phase) recovered from a split femur after 7 days (**Fig. 6E**). This increase in cycling activity also declined until 14 days after transplantation.

We conclude from these observations that the trauma / stress of splitting and transplantation resulted in a loss of haematopoietic cells, after which the system stabilized at a new reduced level.

The fact that haematopoietic activity was retained over the entire lifespan of the transplants, prompted us to investigate, if myeloid progenitor cells were also retained within the haematopoietic compartment of split femurs. Therefore, we recovered the BM 14 days after transplantation and following preparation of single cell suspensions, we probed for the presence of myeloid progenitors by colony formation in semisolid methylcellulose cultures. We identified and enumerated colonies present after one and again 2 weeks of incubation (**Fig. 6F**).

Besides single lineage colonies, we were also able to recover progenitors with multi-lineage potential giving rise to erythroid cells and 3 more myeloid lineages (granulocytes, megakaryocytes and macrophages) from transplanted split femurs (**Fig. 6G**). The colony type distribution was well preserved in split femurs and resembled the wildtype controls more closely than the colony distribution of cells isolated from transplanted whole bones (**Fig. 6F**).

Discussion

While the overall function and general architecture of the BM are well documented, data on the dynamic behavior of different BM cell populations and their complex interrelations are scarce. Powerful new imaging techniques, including multiphoton microscopy, coupled with innovative experimental models promise to overcome the optical limitations imposed by the mineral casing of the femoral marrow. We describe here the development of a novel imaging model for femoral BM that is characterized by the fundamental criterion to allow repetitive *in vivo* observation of BM over broad time intervals of days to weeks, which we refer to as chronic imaging. We designed this model around the well-established dorsal skin-fold chamber (DSC) to provide a stable, contained environment with optical access to an ectopically transplanted, split femur. We imaged this split femur transplant using multiphoton microscopy to acquire information on deeper tissue layers and to burden the sample with lower phototoxicity than that associated with conventional laser scanning microscopy. On average 200 – 300 μm tissue were imaged in the z-dimension independently of the position of imaging along the long axis of the femur.

In a DSC, ectopically transplanted split femurs re-vascularize and continue their development in an age-dependent manner

After transplantation of longitudinally split femurs into a DSC, we persistently noted a gradual erythrocyte accumulation inside the open marrow cavity, starting between 24 and 48hrs after transplantation. Erythrocytes accumulations consistently covered the whole opened marrow cavity 4 d after transplantation. Based on our observations using stereomicroscopy, *intravital* multiphoton microscopy and immunohistology that demonstrated transplant perfusion and development of a progressively sprouting, dense vascular network uniformly covering the femur, we interpreted the presence of hematoma as a consequence of the successful connection between the ectopically transplanted femur and the host vasculature.

As the splitting process will inevitably result in damage to the BM vasculature the most obvious explanation would be that such lesions only healed after reconnection to the host circulation and initial local hemorrhages. We can however not exclude reperfusion-induced damage to the neonate femoral vasculature or the formation of erythrocyte filled lacunae due to strong hypoxia-driven, local erythropoiesis in the absence of vascular connections with the host. After 8 days the transplant vasculature was well perfused and functional as the imaging of contrasting agents did not indicate the existence of vascular lesions (Movie 1).

We hypothesized that femurs collected postnatally would connect faster and have a better chance of adapting to the new environment, compared to tissue collected from adult donors. Multiphoton and immunohistology data however revealed that neonates between P05 and P10 were not suited as donors as the marrow cavity progressively closed with new woven bone and the epiphysis was completely covered by mesenchymal cells. This closing of the BM with new bone decreased with donor age until it was no longer observed in P17 pups. Since all femurs were subjected to identical environmental factors in the DSC, the effect is most likely age-related and results from the early neonatal femur's inability to compensate imbalances caused by ectopic transplantation leading to a random differentiation of progenitor cells toward mesenchymal and bone lineages. Equally plausible, the closing of the marrow cavity could result from progenitor cell

Figure 6 (See previous page). Haematopoietic progenitor cells are retained in split femur transplants although at a low frequency. (**A**) Cryosection demonstrating the population of the secondary ossification center (SOC) of a split femur with haematopoietic cells 14 d after transplantation (3 transplants). (**B**) Genetic tracing reveals the presence of host haematopoietic cells (Ly-EGFP^{+}) in the bone marrow cavity of a transplanted split femur (Tie2-Cre;R26-RFP) 15 d after transplantation. MIP of a multi-photon image stack (2 transplants). (**C**) Cells from the grafted femur, flushed 14 d after transplantation, belong both to the donor (Tie2-Cre; R26-RFP) and to the host (Syk-Cre; R26-YFP) (3 pooled transplants). (**D**) Macrophages and neutrophils decrease most in the interval between transplantation and day 3, then maintain constant levels until the end of experimentation period. For this experiment cells recovered from 3 or 4 transplants per time point were pooled and stained. (**E**) Propidium iodide cell cycle analysis for haematopoietic cells recovered from transplant at several time points show an initial increase in proliferation potential until day 7, that decreases with time until the end of the observation time (n = 3 or 4 transplants per time point). (**F**) Transplanted split femurs retain progenitor cells with myeloid differentiation capacity. Bone marrow cells from split or whole femur transplants were recovered 14 days after transplantation and the myeloid differentiation potential was analyzed in semisolid methylcellulose cultures. Shown is the contribution of the indicated colony types in (%) of the total colony number recovered (100%). Ctrl denotes freshly recovered femoral BM, half transplantation of a split femur, whole transplantation of an intact femur. Days indicate time after seeding at which the identity of the colonies was identified. (control = 5; half split = 20; whole femur = 4) (**G**) Morphology in methylcellulose (top panels) and histological appearance after cytocentrifugation and May–Grünwald-Giemsa staining (bottom panels) of representative colonies grown from cells recovered from transplants. CFU-M: macrophage colony; CFU-G: granulocytic colony, CFU-Mix: multilineage colony.

differentiation aiming to regain the shielded haematopoietic microenvironment. One intermediate phase in fracture repair consists of mesenchymal cell differentiation into osteoblasts, which will fill the gap with woven bone.[18] The age-dependent decline in fracture healing is coupled, among other factors,[19] with a reduced number of stem and progenitor cells[20] and a decreased self-renewal capacity of osteoprogenitors.[21] This is consistent with the smaller surface covered by new bone when we transplanted femurs from donors of increasing ages. Presently, it is not known if the difference in bone healing decreases to this extend between postnatal days 5 and 17 in mice, but in teenagers, the geometric mean of the time required for complete femoral fracture healing increased uniformly by 0.7 wks/ yr.[22] Nevertheless for investigations aiming to study bone development and healing, younger femur transplants might be advantageous.

The split femur gives rise to a new functional vascular network that is morphologically similar to the normal bone marrow vasculature and allows intravital imaging of angiogenic responses

Genetic labeling revealed that endothelial cells (EC) contributing to newly forming BVs in the transplant were almost completely transplant derived, anastomosing with a limited number of BVs that presented host-derived markers. This observation was unexpected, since we anticipated secreted angiogenic growth factors to be released after splitting the femur[23,24] and to induce a strong angiogenic host response. Though multiphoton microscopy allows deep tissue imaging, however in our model, the bone shaft obscured assessment of vascular connections made directly underneath the bone. Therefore, we can presently not comprehensively assess the extent and origin of initial vascular connections between the femur and skin.

Recently, BM EC subtypes have been described based on the expression of the markers PECAM-1 and endomucin (Emcn).[15] The specific EC subtype likely responsible for the revascularization of the split femur is the PECAM-1 and Emcn expressing type H, localized endosteal and metaphyseal and re-establishing the BM BVs after lethal irradiation. Hypoxia was probably not the driving force behind the exuberant sprouting observed from the transplanted split femurs, as the new environment of the DSC offered more access to oxygen through the split and the sprouting continued after the transplant had already connected to the host vasculature and received nutrients.

The venous vascular tree in the normal femur includes a particular type of BV called sinusoidal capillary. BM sinusoids are distinguished from the venous compartment of other organ systems by morphological differences,[25] such as a thicker diameter and frequent branching points. The BVs covering the transplant exhibited a similar, distinct morphology, which was completely different from the skin BVs (i.e. thin with uniform diameter and seldom branching points). A common feature of femoral and transplant vasculature was the presence of vascular loops and openings / discontinuities. Possibly, vascular loops resulted during sprouting angiogenesis, when 2 closely positioned tip cells fused and created a lumen by re-arranging EC−EC contacts.[26] Openings / discontinuities may have been the result of vascular fusion and remodeling, which transiently left transluminal endothelial pillars, before completion of the fusion / remodeling process.[27] Sinusoids are characterized by a thin vascular wall comprised of a thin discontinuous basement membrane and incompletely covered by perivascular cells,[28] that send projections into the BM.[29] We used a genetic model that expressed NG2-DsRed in various cell populations including perivascular cells, and observed that their morphology differed according to their distance to the angiogenic front: the closer $NG2^+$ cells were to the front, the more discontinuous was their coverage of the sprouting BVs and they adopted a more active phenotype with filopodia extending into the environment. At the newly-formed vascular plexus contrasting agents showed no increased vascular leakage, suggesting that the new vessels were stable, likely also due to the stabilizing effect of perivascular cells.[30]

Split femurs retain myeloid progenitor cells at a low level: a model for reactive or stressed hematopoiesis?

Within the first 3 days after transplantation, we noted a rapid loss in haematopoietic cellularity contained in split femurs, followed by a stabilization or even small recovery in transplant-derived haematopoietic cell numbers that coincided with a small increase in the frequency of cycling cells. Although hematopoiesis never recovered to the initial levels, the stabilization of the haematopoietic cell complement and the fact that myeloid progenitor cells were retained in the split femur throughout the duration of the experiment suggested that a basal level of bone marrow function was preserved after transplantation.

This makes the model potentially useful to investigate regenerative or reactive stress hematopoiesis and distinct, albeit rare, homing events. Quantification of the myeloid differentiation potential in the transplants revealed a skewing toward the granulocytic lineage, compared to cells retrieved from age-matched controls. The trauma and damage of the splitting process, but also the strong angiogenic response of the transplant likely disturbed the normal BM niche, through displacement of stromal cells and changes in the ratio of EC to other stromal cells due to extensive angiogenesis. Interestingly, the differentiation profile of cells from a split femur was closer to control BM than the profile of cells retrieved from an intact transplanted femur, suggesting that oxygen availability to the haematopoietic compartment apparently was sufficient in split femurs. The presence of host cells within the transplant, revealed by genetic labeling, deserves further investigation as it could be indicative of reparatory/ healing processes or even a partial repopulation of the transplant by circulating host progenitor cells.

In conclusion, we have created a novel imaging model that allows sustainable direct, which we call chronic, optical access to femoral BM (see supplemental **Fig. 4S**). Our approach relied on the rapid and efficient vascularization of a split femur transplanted into a dorsal skin chamber, which had been surgically implanted on the back of a mouse. In this setting, multiphoton microscopy allowed analysis of the angiogenic behavior of BM ECs. We noted a striking resemblance of vessels sprouting after transplantation and BM sinusoids, suggesting that in this model typical parameters of the BM EC are likely retained. Split femur transplants

maintained a basal level of various haematopoietic cells of the myeloid differentiation hierarchy thus pointing toward being suitable as a model for regenerative or stress hematopoiesis. Furthermore it fosters the hope that the sustained presence of progenitor cells will ultimately allow the direct observation and analysis of cellular interactions between haematopoietic cells, either donor or host -derived and the bone marrow niche.

Experimental procedures

Mice

All animal experiments were approved by the Animal Experimentation Committee of the county of Münster and the Federal Ministry of Nature, Environment and Consumer Protection, North Rhine Westphalia. All genetic models were used on the background of: C57Bl/6 (Janvier); the strains were Syk-Cre[17]; LifeAct-GFP/ -RFP;[31] LyEGFP;[32] NG2-DsRed;[33] R26R-tdRFP;[34] R26-YFP;[35] Tie2-Cre (Jackson Laboratory, 004128).

Dorsal skinfold chamber implantation and femur transplantation

The implantation procedure was performed as described in literature,[12,36] with some modifications. In short, DSC implantation consisted of sandwiching the dorsal skin between 2 titanium plates and then removing a circular skin portion the size of the observation window, before closing the chamber. Femurs were split after fixation either in a custom parallel vice or using watchmaker forceps on the lid of a 50ml Falcon tube using a fresh surgical disposable scalpel (B.Braun, Aesculap cutfix stainless scalpel #11). Split femurs were transplanted on the third day after chamber implantation, first to exclude chambers showing inflammation or bleeding and second to allow completion of wound healing thus minimizing the influence of wound healing on the observed processes in the open femoral marrow.

In vivo imaging using multiphoton microscopy

The multiphoton system consisted of a modified upright stage Olympus, BX51WI, equipped with a Chameleon XR laser system (Coherent), optical parametric oscillator (A.P.E.-Berlin), TriMScope scan head (LaVision BioTec GmbH), GaAsP NDD detectors (Hamamatsu, H7244a-40), and an immersion XLumPlanFl, 20 × 0.95 NA, W/IR Objective (Olympus). Images were acquired using ImSpector software (LaVisionBioTech). A Univentor 400 pump (TSE Systems) was used to control an isoflurane anesthesia mix of carrier gas (air enriched with oxygen, 250–300 mL/h) and anesthetic (isoflurane: induction 2–2.5%, maintenance 0.7–1.2%). Mice were immobilized in a custom-made holder that fitted the implanted DSC and allowed prevention of hypothermia by body temperature maintenance using a HAAKE DC10-K10 (Thermo) heating circulator. Eyes were covered with protection crème.

Contrasting agents, stains and antibodies

FITC-dextran (2 MDa, Sigma 152251), TexasRed-dextran (70 kDa life-technologies D1830). Quantum dots Macoun Red (Evident Technologies), Hoechst 33342 (Molecular Probes H3570). αCD16/32 (clone 2.4G2, BD PharMingen, 553140), αCD3ε-FITC (clone 145-2C11, BD PharMingen, 553062), αLy6G-PE (clone 1A8, BD PharMingen, 551461), αF4/80 (clone CI:A31, AbD Serotec, MCA497).

Immunofluorescence staining

Tissue was cut into small pieces and fixed in 4% neutral buffered PFA. After washing and cryoprotection in glycerol solutions of increasing concentration (10%, 30% and 60%), samples were embedded in OCT or bone embedding medium (8% gelatine + 1% PVP). Embedded pieces were frozen in a dry ice / isopentane slurry. Thin (10 μm) and thick (50–80μm) tissue sections were rehydrated with warm PBS, and incubated in PermBlock for 2 h (1% BSA (w/v) 0.1% Tween-20 (v/v) in PBS) for weaker block or 3% BSA (w/v) and 0.5% (v/v) Tween-20 in PBS for stronger block). Sections were incubated with primary antibodies in PermBlock overnight at 4°C, followed by 3 10 min washes in PBS-T. Incubation with secondary antibodies for 4 h at 4°C was followed by 3 washes in PBS-T, the last one containing Hoechst 33258 (1:10.000 for 30 min). After three final washes samples were mounted in Mowiol.

Isolation of bone marrow single cell suspensions

BM was harvested by flushing femurs with a 1 mL syringe (27 G needle) with supplemented culture medium or FACS buffer (3% BSA in PBS). Cells of transplants were gently flushed with supplemented culture medium into a 3 cm petri dish. In all cases, the resulting suspensions were passed through cell filters (e.g., CellTrics) to obtain a single cell suspension.

Colony forming unit assay

Murine BM cells were collected from transplanted femurs 14 days after transplantation or from age matched mice and sedimented at 300 × g (4°C). Cells were plated in 35 mm culture dishes with semi-solid culture medium comprised of IMDM containing 1% (w/v) methylcellulose, 10% heat-inactivated fetal bovine serum, 5% deionized and delipidated BSA, 1.5% IL-3 conditioned medium, 200 μg/mL iron-saturated transferrin, 25 μg/mL dipalmitoyl choline, cholesterol and oleic acid, 5 U/mL Epo, 10 μg/mL rh insulin, 12.5 ng/mL rm SCF, 10 ng/mL rh IL-6, 1 mM β-mercaptoethanol and 15% of 5637-cell conditioned medium. Type and frequency of colonies comprised of more than 50 cells were enumerated after 7 day or 14 day incubation (37°C, 5% CO2). Correct identification of colonies was confirmed by phase-contrast microscopy of May-Grünwald Giemsa stained cytospin preparations.

Image processing

All images were processed using either Imaris (Bitplane) or Fiji31 software. To enhance overall features, linear enhancement of brightness and contrast was performed homogenously on whole images. 3D architecture of the new vascular

beds was depicted using the Temporal-Color Code plugin in Fiji.[37]

Disclosure of Potential Conflicts of Interest

No potential conflicts of interest were disclosed.

Acknowledgments

We thank Markus Sperandio (Munich) for invaluable training and advice on using the dorsal skin fold chamber, R Erepaneedi and members of the Vestweber department for discussion and reagents, S Volkery, M Stehling, L Kremer, N Kümpel-Rink and B Waschk for technical assistance.

Funding

This work was supported by a fellowship of the International Max Planck Research School - Molecular Biomedicine (IMPRS-MBM) and a CiM (DFG EXC 1003 Cells in Motion) Bridging Fellowship to MB and grants from the Deutsche Forschungsgemeinschaft (SFB 629, SFB656) and the Max Planck Society to FK.

Supplemental Material

Supplemental data for this article can be accessed on the publisher's website.

Reference

1. Ramasamy SK, Kusumbe AP, Adams RH. Regulation of tissue morphogenesis by endothelial cell-derived signals. Trends Cell Biol. 2015; 25 (3):148-57; PMID:25529933; http://dx.doi.org/10.1016/j.tcb.2014.11.007
2. Travlos GS. Histopathology of bone marrow. Toxicol. Pathol. 2006; 34 (5):566-98; PMID:17067944; http://dx.doi.org/10.1080/01926230600964706
3. Kohler A, Schmithorst V, Filippi MD, Ryan MA, Daria D, Gunzer M, Geiger H. Altered cellular dynamics and endosteal location of aged early hematopoietic progenitor cells revealed by time-lapse intravital imaging in long bones. Blood 2009; 114 (2):290-8; PMID:19357397; http://dx.doi.org/10.1182/blood-2008-12-195644
4. Sipkins DA, Wei X, Wu JW, Runnels JM, Cote D, Means TK, Luster AD, Scadden DT, Lin CP. In vivo imaging of specialized bone marrow endothelial microdomains for tumour engraftment. Nature 2005; 435 (7044):969-73; PMID:15959517; http://dx.doi.org/10.1038/nature03703
5. Lo Celso C, Fleming HE, Wu JW W, Zhao CX, Miake-Lye S, Fujisaki J, Cote D, Rowe DW, Lin CP, Scadden DT. Live-animal tracking of individual haematopoietic stem/progenitor cells in their niche. Nature 2009; 457 (7225):92-U96; PMID:19052546; http://dx.doi.org/10.1038/nature07434
6. Boyerinas B, Zafrir M, Yesilkanal AE, Price TT, Hyjek EM, Sipkins DA. Adhesion to osteopontin in the bone marrow niche regulates lymphoblastic leukemia cell dormancy. Blood 2013; 121 (24):4821-31; PMID:23589674; http://dx.doi.org/10.1182/blood-2012-12-475483
7. Lassailly F, Foster K, Lopez-Onieva L, Currie E, Bonnet D. Multimodal imaging reveals structural and functional heterogeneity in different bone marrow compartments: functional implications on hematopoietic stem cells. Blood 2013; 122 (10):1730-40; PMID:23814020; http://dx.doi.org/10.1182/blood-2012-11-467498
8. Sckell A, Leunig M. The dorsal skinfold chamber: studying angiogenesis by intravital microscopy. Methods Mol. Biol. 2009; 467:305-17; PMID:19301680; http://dx.doi.org/10.1007/978-1-59745-241-0_19
9. Leunig M, Yuan F, Gerweck LE, Jain RK. Effect of basic fibroblast growth factor on angiogenesis and growth of isografted bone: quantitative in vitro-in vivo analysis in mice. Int. J. Microcirc. Clin. Exp. 1997; 17 (1):1-9; PMID:9176719; http://dx.doi.org/10.1159/000179199
10. Leunig M, Yuan F, Berk DA, Gerweck LE, Jain RK. Angiogenesis and growth of isografted bone: quantitative in vivo assay in nude mice. Lab Invest 1994; 71 (2):300-7; PMID:7521447
11. Leunig M, Demhartner TJ, Sckell A, Fraitzl CR, Gries N, Schenk RK, Ganz R. Quantitative assessment of angiogenesis and osteogenesis after transplantation of bone: comparison of isograft and allograft bone in mice. Acta Orthop. Scand. 1999; 70 (4):374-80; PMID:10569268; http://dx.doi.org/10.3109/17453679908997827
12. Sckell A, Leunig M. Dorsal skinfold chamber preparation in mice : studying angiogenesis by intravital microscopy. Methods Mol. Med. 2001; 46:95-105; PMID:21340915
13. Oka M, Kubota S, Kondo S, Eguchi T, Kuroda C, Kawata K, Minagi S, Takigawa M. Gene expression and distribution of connective tissue growth factor (CCN2/CTGF) during secondary ossification center formation. J Histochem Cytochem 2007; 55 (12):1245-55; PMID:17875658; http://dx.doi.org/10.1369/jhc.7A7263.2007
14. Kuhn A, Brachtendorf G, Kurth F, Sonntag M, Samulowitz U, Metze D, Vestweber D. Expression of endomucin, a novel endothelial sialomucin, in normal and diseased human skin. J Investig Dermatol 2002; 119 (6):1388-93; PMID:12485444; http://dx.doi.org/10.1046/j.1523-1747.2002.19647.x
15. Kusumbe AP, Ramasamy SK, Adams RH. Coupling of angiogenesis and osteogenesis by a specific vessel subtype in bone. Nature 2014; 507 (7492):323-+; PMID:24646994; http://dx.doi.org/10.1038/nature13145
16. Armulik A, Genove G, Mae M, Nisancioglu MH, Wallgard E, Niaudet C, He L, Norlin J, Lindblom P, Strittmatter K, Johansson BR, Betsholtz C. Pericytes regulate the blood-brain barrier. Nature 2010; 468 (7323):557-61; PMID:20944627; http://dx.doi.org/10.1038/nature09522
17. Bohmer R, Neuhaus B, Buhren S, Zhang D, Stehling M, Bock B, Kiefer F. Regulation of developmental lymphangiogenesis by Syk(+) leukocytes. Dev. Cell 2010; 18 (3):437-49
18. Brighton CT, Hunt RM. Early histological and ultrastructural changes in medullary fracture callus. J. Bone Joint Surg. Am. 1991; 73 (6):832-47; PMID:2071617
19. Lu CY, Hansen E, Sapozhnikova A, Hu D, Miclau T, Marcucio RS. Effect of age on vascularization during fracture repair. J Orthop Res 2008; 26 ((10):1384-9; PMID:18464248; http://dx.doi.org/10.1002/jor.20667
20. Nishida S, Endo N, Yamagiwa H, Tanizawa T, Takahashi HE. Number of osteoprogenitor cells in human bone marrow markedly decreases after skeletal maturation. J Bone Miner Metab 1999; 17 (3):171-7; PMID:10757676; http://dx.doi.org/10.1007/s007740050081
21. Bellows CG, Pei W, Jia Y, Heersche JN. Proliferation, differentiation and self-renewal of osteoprogenitors in vertebral cell populations from aged and young female rats. Mech. Ageing Dev. 2003; 124 (6):747-57; PMID:12782418; http://dx.doi.org/10.1016/S0047-6374(03)00088-5
22. Skak SV, Jensen TT. Femoral shaft fracture in 265 children. Log-normal correlation with age of speed of healing. Acta Orthop. Scand. 1988; 59 (6):704-7; PMID:3213461; http://dx.doi.org/10.3109/17453678809149430
23. Harada S, Nagy JA, Sullivan KA, Thomas KA, Endo N, Rodan GA, Rodan SB. Induction of vascular endothelial growth factor expression by prostaglandin E2 and E1 in osteoblasts. J. Clin. Invest 1994; 93 (6):2490-6; PMID:8200985; http://dx.doi.org/10.1172/JCI117258
24. Fuchs S, Baffour R, Zhou YF, Shou M, Pierre A, Tio FO, Weissman NJ, Leon MB, Epstein SE, Kornowski R. Transendocardial delivery of autologous bone marrow enhances collateral perfusion and regional function in pigs with chronic experimental myocardial ischemia. J Am College Cardiol 2001; 37 (6):1726-32; PMID:11345391; http://dx.doi.org/10.1016/S0735-1097(01)01200-1
25. Kopp HG, Hooper AT, Avecilla ST, Rafii S. Functional Heterogeneity of the Bone Marrow Vascular Niche. Hematopoietic Stem Cells Vii 2009; 1176:47-54
26. Lenard A, Ellertsdottir E, Herwig L, Krudewig A, Sauteur L, Belting HG, Affolter M. In vivo analysis reveals a highly stereotypic morphogenetic pathway of vascular anastomosis. Dev. Cell 2013; 25 (5):492-506
27. Chouinard-Pelletier G, Jahnsen ED, Jones EA. Increased shear stress inhibits angiogenesis in veins and not arteries during vascular development. Angiogenesis 2013; 16 (1):71-83; PMID:22941228; http://dx.doi.org/10.1007/s10456-012-9300-2
28. Inoue S, Osmond DG. Basement membrane of mouse bone marrow sinusoids shows distinctive structure and proteoglycan composition: A high resolution ultrastructural study. Anatomical Record 2001; 264 (3):294-304; PMID:11596011; http://dx.doi.org/10.1002/ar.1166
29. Weiss L. The hematopoietic microenvironment of the bone marrow: an ultrastructural study of the stroma in rats. Anat. Rec. 1976; 186 (2):161-84; PMID:984472; http://dx.doi.org/10.1002/ar.1091860204
30. Murfee WL, Skalak TC, Peirce SM. Differential arterial/venous expression of NG2 proteoglycan in perivascular cells along microvessels: Identifying a venule-specific phenotype. Microcirculation 2005; 12 (2):151-60; PMID:15824037; http://dx.doi.org/10.1080/10739680590904955
31. Riedl J, Flynn KC, Raducanu A, Gartner F, Beck G, Bosl M, Bradke F, Massberg S, Aszodi A, Sixt M, Wedlich-Soldner R. Lifeact mice for studying F-actin dynamics. Nature Methods 2010; 7 (3):168-9; PMID:20195247; http://dx.doi.org/10.1038/nmeth0310-168
32. Faust N, Varas F, Kelly LM, Heck S, Graf T. Insertion of enhanced green fluorescent protein into the lysozyme

gene creates mice with green fluorescent granulocytes and macrophages. Blood 2000; 96 (2):719-26; PMID:10887140

33. Zhu XQ, Bergles DE, Nishiyama A. NG2 cells generate both oligodendrocytes and gray matter astrocytes. Development 2008; 135 (1):145-57; PMID:18045844; http://dx.doi.org/10.1242/dev.004895
34. Luche H, Weber O, Rao TN, Blum C, Fehling HJ. Faithful activation of an extra-bright red fluorescent protein in "knock-in" Cre-reporter mice ideally suited for lineage tracing studies. Eur J Immunol 2007; 37 (1):43-53; PMID:17171761; http://dx.doi.org/10.1002/eji.200636745
35. Srinivas S, Watanabe T, Lin CS, William CM, Tanabe Y, Jessell TM, Costantini F. Cre reporter strains produced by targeted insertion of EYFP and ECFP into the ROSA26 locus. BMC. Dev. Biol. 2001; 1:4; PMID:11299042; http://dx.doi.org/10.1186/1471-213X-1-4
36. Palmer GM, Fontanella AN, Shan SQ, Hanna G, Zhang GQ, Fraser CL, Dewhirst MW. In vivo optical molecular imaging and analysis in mice using dorsal window chamber models applied to hypoxia, vasculature and fluorescent reporters. Nat Protocols 2011; 6 (9):1355-66; PMID:21886101; http://dx.doi.org/10.1038/nprot.2011.349
37. Schindelin J, Arganda-Carreras I, Frise E, Kaynig V, Longair M, Pietzsch T, Preibisch S, Rueden C, Saalfeld S, Schmid B, Tinevez JY, White DJ, Hartenstein V, Eliceiri K, Tomancak P, Cardona A. Fiji: an open-source platform for biological-image analysis. Nat Methods 2012; 9 (7):676-82; PMID:22743772; http://dx.doi.org/10.1038/nmeth.2019